Gonzalez-Vogel, Alvaro; Felis-Carrasco, Francisco; Rojas, Orlando J.

3D printed manifolds for improved flow management in electrodialysis operation for desalination

Published in:
Desalination

DOI:
10.1016/j.desal.2021.114996

Published: 01/06/2021

Document Version
Publisher's PDF, also known as Version of record

Desalination 505 (2021) 114996

Contents lists available at ScienceDirect

Desalination

journal homepage: www.elsevier.com/locate/desal

3D printed manifolds for improved flow management in electrodialysis operation for desalination

Alvaro Gonzalez-Vogel [a,b,*], Francisco Felis-Carrasco [d], Orlando J. Rojas [b,c]

[a] Bioforest S. A., Camino Coronel Km 15, VIII, Region, Chile
[b] Department of Bioproducts and Biosystems, School of Chemical Engineering, Aalto University, Finland
[c] Bioproducts Institute, Departments of Chemical and Biological Engineering, Chemistry and Wood Science, University of British Columbia, 2360, East Mall, Vancouver, BC, V6T 1Z3, Canada
[d] Dantec Dynamics A/S, Skovlunde, Denmark

HIGHLIGHTS

- Manifolds were 3D printed for improving water flow distribution in electrodialysis.
- New flow inter-connectivity is possible when using 3D printing.
- The even distribution of water flow allows an increased limiting current density.
- New functionalities can be integrated in desalination equipment.
- Desalination cost is decreased if the manifold geometry is correctly adapted.

ARTICLE INFO

Keywords:
3D printing
Manifold electrodialysis
Multifunctional frame
Additive manufacturing
Desalination

ABSTRACT

Desalination with electrodialysis requires cell designs for optimal flow distribution. Such units include polymeric frames, electrodes, membranes and spacers. Frames are used for mechanical support of electrodes and hydraulic connectors. Their geometry needs to be customized for appropriate fluid management and hydraulic compartmentalization. Typically, such electrodialysis frames are manufactured by drilling solid plastic blocks. However, design flexibility is required to fit the increasing number of developments incorporating new materials and flow inter-connectivity. Here we propose additive manufacturing coupled with computational design to optimize flow dynamics and their coupling with physical devices. First, CAD models are proposed to incorporate major improvements in process lines, and to integrate internal manifold cavities. Even fluid flow and pressure drop distributions are verified by numerical models at given flowrates. The frames were 3D printed and assembled with electrodes and membranes to investigate their performance, and to experimentally confirm numerical predictions. Compared to conventional frames, and as a result of the even distribution of the fluids inside the cell, it was possible to reach an improved (21% higher) limiting current density while ensuring pH stability. Finally, our approach can be integrated in new designs, taking advantage of material selection and geometrical complexity of 3D-printing to add novel functionalities.

1. Introduction

3D printing or additive manufacturing offers a high potential in design and engineering [1]. This is due to the possibility of fabricating components with complex geometries and integrating materials with multiple functions. Moreover, it is an affordable technology that makes it easy to materialize designed prototypes [2].

The applicability of 3D printed units for water management, for example, in desalination and wastewater treatment, is gaining increased attention as it has been reported for the development of spacers that fit separators [3–5] and membranes [6]. The optimization of such spacers in all membrane-based processes can reduce fouling by effectively promoting turbulence on the surface of those membranes, consequently decreasing energy consumption and limiting the need for chemical

* Corresponding author at: Bioforest S. A., Camino Coronel Km 15, VIII, Region, Chile.
E-mail address: alvaro.gonzalez.v@arauco.com (A. Gonzalez-Vogel).

https://doi.org/10.1016/j.desal.2021.114996
Received 5 October 2020; Received in revised form 8 January 2021; Accepted 30 January 2021
Available online 25 February 2021

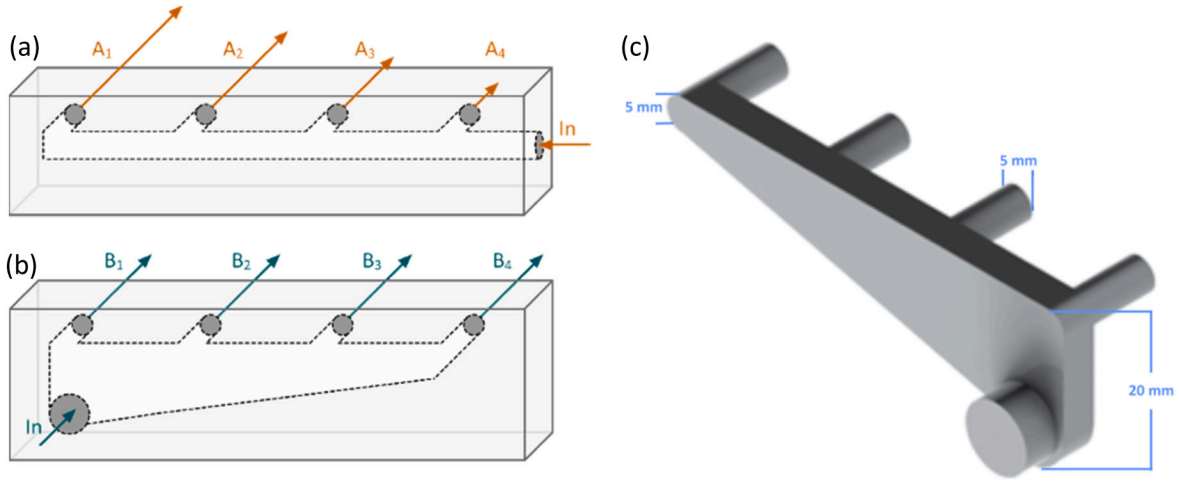

Fig. 1. Flow distribution and manifold design. The arrows represent the direction of input and output streams. (a) Distribution of the sample in conventional electrodialysis frames (control ED). (b) Flow distribution using a manifold cavity. (c) 3D representation of the used distribution system.

treatments, such as those used for cleaning and system regeneration [3].

In these efforts, electrodialysis (ED) has emerged as a membrane-based technique that is able to separate ions from aqueous solutions. In conventional ED, a solution is pumped through a cell, which contains alternated anion and cation exchange membranes between a couple of electrodes. Under the applied electrical potential ion transport occurs, thereby dialyzing the incoming solution and concentrating the removed salts in alternated hydraulic streams. Hence, a main application of ED is water desalination [7].

Since their introduction, 3D printed components for electrodialysis systems have not experienced major developments. Main research efforts have focused on membrane improvement [8–10] and design of spacers [11]. However, to our knowledge, no commercial development have been reported to manufacture ED components via 3D printing. This is surprising since 3D printing offers an unexploited potential to produce and integrate modular components that can afford intricate geometries, such as valves, pumps, filters, frames, connectors, sensors, and even electrodes. Such possibilities can add new or multiple functions to ordinary designs and may decrease manufacturing costs of ED.

In this work, we designed and materialized a multifunctional electrodialysis cell frame using Fused Deposition Modelling (FDM). Incorporation of internal manifolds for an even distribution of the fluids helped to stabilize the desalination process, increasing the reached limiting current density (LCD) and stabilizing the pH of operation. As a result, a new multifunctional component for electrodialysis is proposed, taking advantage of complex structures obtained by additive manufacturing.

2. Materials and methods

2.1. Chemicals & membranes

NaCl and Na_2SO_4 (analytical grade) were obtained from Merck Chemicals. Standard desalination anionic exchange membranes (PC-SA) and cationic exchange membranes (PC-SK) were purchased from PCCell GmbH, Germany. PC-SA and PC-SK have an electrical resistance of 1.8 and 2.5 Ω/cm^2 respectively.

2.2. Electrodialysis experiments

The ED system including power supply, pumps, automatic valves, and electrodialysis cell ED64 consisted of a commercial laboratory-scale unit acquired from PCCell GmbH, Germany. Five pairs of ion exchange membranes provided a total surface area of 640 cm^2 (individual membrane area of 64 cm^2). The flow rate was fixed at 30 l/h, with a linear flow velocity of 2.08 cm/s, considering spacers with a thickness of 0.05 cm and an effective area of 64 cm^2. The rinsing compartment of electrodes incorporated a 0.25 M Na_2SO_4 aqueous solution with a flow of 1.2 l/min [12]. The solutions were kept at 20 °C by using an external water jacket. The variation of flowrate was only at model scale, to calculate the Reynolds number for all simulation cases.

2.3. 3D-printing of the frame

Software 123D Design (v 2.1.11) from Autodesk was employed for CAD (Computer-Aided Design) modelling of the cell frame. The software Slic3r (v 1.2.9) was utilized for generating a G-Code which was run by a desktop 3D printer PRUSA i3, using Fused Deposition Modelling technology. PETG filament with a diameter of 1.75 mm was chosen due to its chemical resistance, thermal stability, and good mechanical strength. The basic parameters used for printing were: 0.1 mm of resolution, 3 mm for all the perimeters, 50% of rectilinear infill, no support material, a maximum print speed of 60 mm/s, 250 °C for the first layer, 238 °C for the other layers and 60 °C for the heating bed.

2.4. Limiting current density determination

The LCD was determined using empirical data. A plot of electrical resistance of the membrane stack (Ohm's Law, Eq. (1)) plotted against the reciprocal value of current was used [16]. The inflection point of the curve indicates the reached LCD.

$$Stack\ Resistance\ (\Omega) = V/I \tag{1}$$

where V in the stack voltage and current, respectively. A 1000 ppm NaCl solution, with an initial pH of 6.8 and a conductivity of 1995 μS/cm, was used to determine the LCD.

3. Results and discussion

3.1. Manifold design

One of the main parameters that affects the operation of electrodialysis system is the limiting current density (LCD). This value is reached when the ions are depleted from the surface of the membranes while desalting [13]. LCD not only limits the operation of the process but is important in mineral scaling on the membranes, which is usually triggered by pH swings in the compartments as a consequence of water splitting. LCD is affected by multiple factors, such as ion concentration,

Table 1
Boundary conditions.

	Velocity u_i	Pressure P
Inlet	*Uniform* profile from Flow rates in Table 2.	*zeroGradient*
Wall	$u_i = 0$ (no slip)	*zeroGradient*
Outlet	*zeroGradient*	$P = 0$

Table 2
Reynolds number for all simulation cases considered on both, control electrodialysis frame (Control ED) and designed manifold.

Flow rate Q (l/h)	*Re* control ED (d_{in} = 7 mm)	*Re* manifold (d_{in} = 10 mm)
10	459	321
20	918	643
30	1377	964
40	1837	1286
50	2296	1607

temperature, architecture of spacers and hydrodynamic conditions [14]. High flowrates ensure a good turbulence and mass transfer of the ions on the membranes surface and, consequently, increasing the current limits [15]. An uneven distribution of the feed solution can lead to LCD values that are reached locally, at given zones of the membranes and long before the rest of the system. Therefore, the efficiency of electrodialysis is expected to be improved if a uniform distribution of hydraulic flows inside the cell is ensured. To this end, the feed flow should be distributed equally across the cell and throughout all the compartments. In this study, we propose the integration of a manifold cavity in the plastic frame, as shown in Fig. 1. More details about the integration in the plastic frame are shown in Section 3.3.

To compensate the pressure losses inside the manifold, its geometry contemplates the input side with a height of 4 times the output diameter (20 mm), decreasing the height of the structure down to 1 time the output diameter at the other end, obtaining a triangular shape (Fig. 1c). Output flowrates were modeled before the experimental tests, to evaluate if a more even flow distribution is achieved in the new manifold compared with the conventional design.

3.2. Modelling of hydrodynamic behaviors

A numerical model was developed using OpenFOAM® v6.0 to study the incompressible laminar flow inside the manifold. The fluid considered for the simulation was pure water at 20 °C, with a kinematic viscosity approximated to $\nu = 1.1 \times 10^{-6} m^2/s$. The numerical model solves the incompressible Navier-Stokes equations to describe the 3D flow inside the Manifolds. The system of equations to solve is the following.

$$\frac{\partial u_i}{\partial t} + u_j \cdot \frac{\partial u_i}{\partial x_j} = -\frac{\partial P}{\partial x_i} + \frac{\partial}{\partial x_j}\left[\nu\left(\frac{\partial u_i}{\partial x_j} + \frac{\partial u_j}{\partial x_i}\right)\right]; \quad (2)$$

$$\frac{\partial u_i}{\partial x_i} = 0; \quad (3)$$

where u_i is the velocity vector in cartesian coordinates in m/s and P the pressure field in m^2/s^2, which is simply expressed as the pressure field p in Pa over the density ρ. The boudary specified for each variable are listed in Table 1.

Two family cases were considered, whereby given flowrates were used for modelling. A control case using the conventional electrodialysis frame is shown in Fig. 1a, and the designed manifold is shown un Fig. 1b. The study cases were chosen based on the limits of the commercial equipment (ED64) employed in the study at laboratory scale, those cases are summarized in Table 2.

After calculating the Reynolds number for each case ($Re = 4Q/\nu d_{in}$) the SIMPLE solver was used to apply a Cartesian 3D steady-state Navier-Stokes equations inside the manifold model. A mesh convergence test was first performed, leaving the analyzed results over an arbitrary 6×10^{-5} tetra-elements mesh. Convergence was attained after ~600 iteration steps with residuals $\varepsilon_{U,P} \leq 10^{-7}$ for the cases at 10, 20 and 30 l/h inlet flowrates. However, as Table 2 shows, both cases present a Reynolds number (*Re*) high enough to produce local instabilities inside the tight turns, when 40 and 50 l/h are used at the injection inlet. In these special cases, a laminar transient approach was used to solve the velocity field, yielding a global solution in a time series. This effect is illustrated in Fig. 2, where the output flowrates for both cavities at 50 l/h are plotted against time. The final result from each simulation case are the Reynolds averaged or time-averaged 3D velocity field $\overline{u}_i$, in the Cartesian (x, y, w) coordinates, and the pressure field $\overline{p}$.

The final metric of the study-cases are the flowrate of every outlet in both systems. To ilustrate the difference of the flow structure produced inside both type of cavities, Fig. 3 shows a combination of the velocity field magnitude (colored) and the streamlines produced from the inlet. For this a Runge-Kutta forward integration in time was used for the streamlines path calculation.

Although a more detailed study of the flow patterns produced inside both devices might be needed, in terms of the type of instabilities generated at relatively high Reynolds numbers (transition to turbulence only when $Re > 2300$ for a circular pipe), some fundamental differences can be extracted from the results shown in Fig. 3 for all the studied flowrates. The distribution of the outlet flowrates is presented in Table 3, using the numbering from the previous Fig. 1 for each case.

After corroborating that the internal manifold could improve the

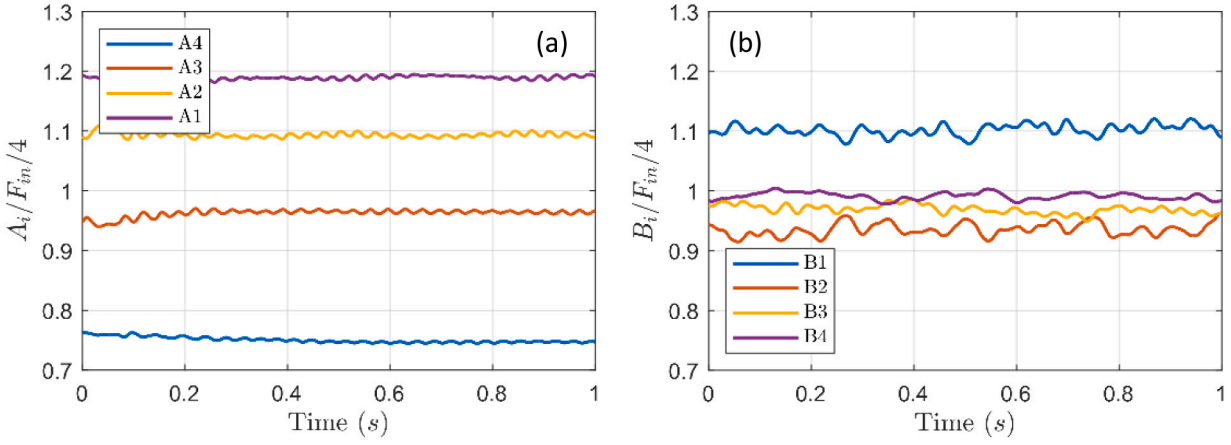

Fig. 2. Output flowrate relative to the perfect 1/4 repartition at 50 l/h in (a) Control case; and (b) Manifold case. Both cases used the numbering from Fig. 1, where A_1 to A_4 refers to the output of the control case, while B_1 to B_4 refers to the output when including the manifold.

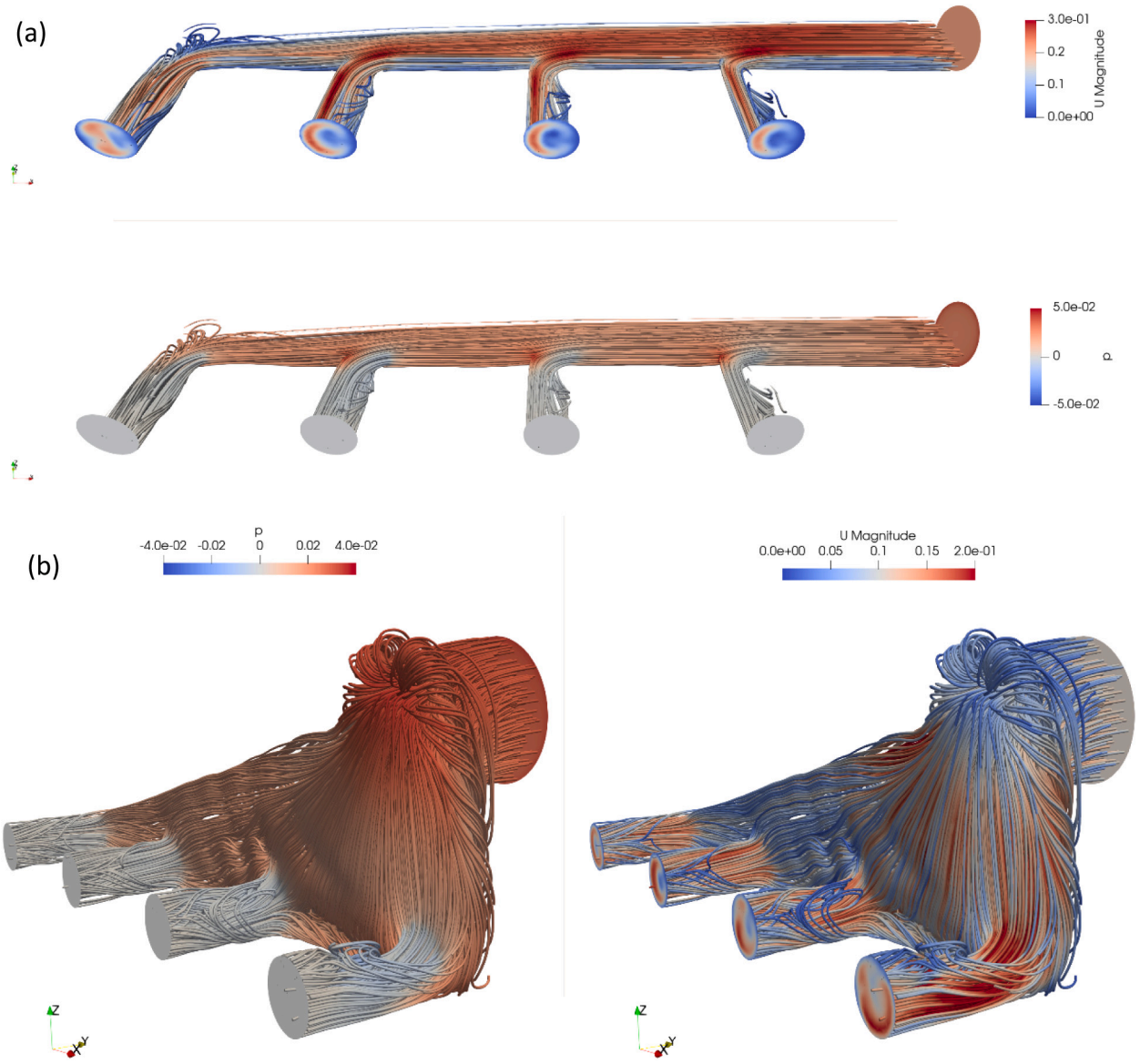

Fig. 3. Streamlines, pressure field in m^2/s^2, and magnitude of the velocity field in m/s for the control case (a), and designed manifold (b). Simulation cases with a flowrate of 30 l/h at the inlet.

Table 3
Flow distribution at different inlet flowrates in the Control cavity. A_1 to A_4 refers to the output of the control case shown in Fig. 1a. B_1 to B_4 refers to the output of the manifold case shown in Fig. 1b.

l/h	Flowrate in outputs of control manifold					Flowrate in outputs of new manifold				
	A_1	A_2	A_3	A_4	A_1/A_4	B_1	B_2	B_3	B_4	B_1/B_4
10	2.8	2.6	2.4	2.2	1.3	3.0	2.5	2.5	2.2	1.4
20	5.8	5.4	4.8	4.1	1.4	5.7	4.8	4.8	4.7	1.2
30	8.7	8.2	7.1	5.9	1.5	8.6	7.1	7.1	7.2	1.2
40	11.9	11.0	9.4	7.7	1.5	11.3	9.3	9.6	9.8	1.2
50	14.9	13.7	12.1	9.3	1.6	13.8	11.7	12.1	12.4	1.1

flow distribution in the electrodialysis frame above 20 l/h, as confirmed with the hydrodynamic models when considering the ratio between opposite outputs. The unit was manufactured for further testing.

3.3. Cell frame design and manufacturing

A 3D model of the frame was generated to fit the actual unit, including manifolds in all the compartments for even distributions of the streams. Post-treatment of the frame was necessary to avoid infiltration of water. When adding layer-by-layer the PETG filaments, small gaps in between them could remain, which facilitate water percolation. An annealing at 80 °C for 2 h sealed the frame, preventing such effects. Nevertheless, the utilization of other filaments, higher degree of infill, or stereolithography printing technique are expected to prevent water leakage and any necessary post-treatment.

The 3D-printed unit resulted in a light frame given the 50% infill

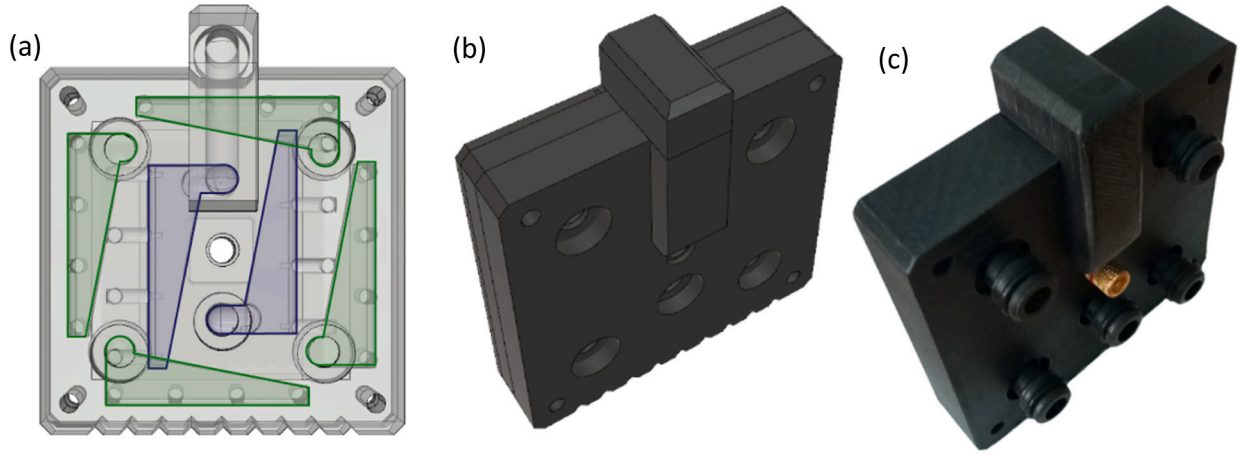

Fig. 4. Designed and built electrodialysis frame. (a) Transparent view of the frame, the internal manifold and holes are observed, in green the manifolds that feed the working compartments, in blue the manifolds of the electrode compartment. (b) Solid representation of the frame, (c) Printed frame and integrated fittings.

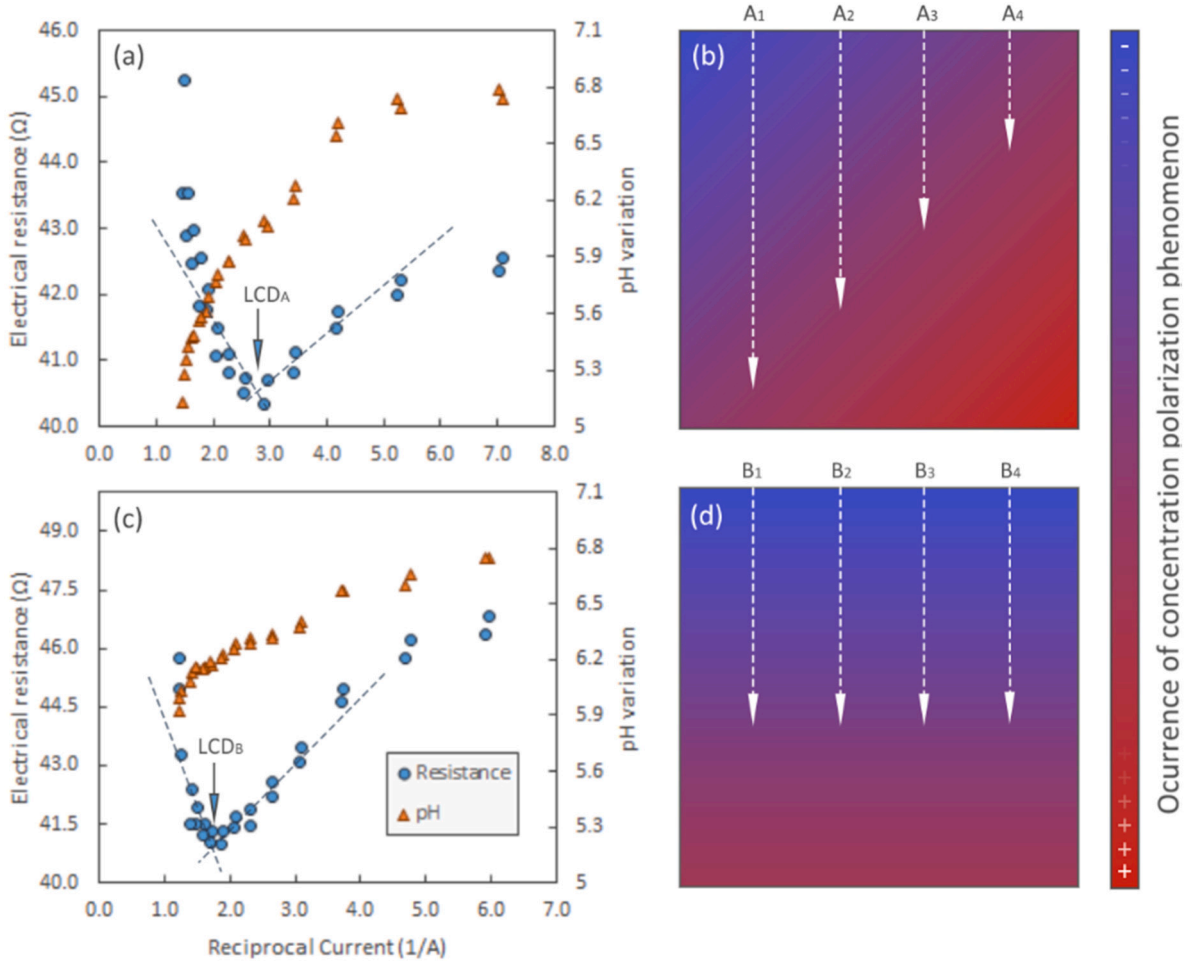

Fig. 5. Limiting Current Density at 30 l/h. (a) Determined LCD and pH variation using conventional frames. (b) Schematic representation of flowrate through the conventional ED cell. (c) LCD and pH variation using the printed frames. (d) Representation of flowrate crossing the printed frames.

employed. After sealing post-treatments, the electrodes plates, banana plug connectors, and fittings were included in the frame, as illustrated in Fig. 4.

3.4. Electrodialysis performance

The uneven distribution of flowrates may promote concentration polarization in some areas of the membranes. At low flowrates the ions on the surface of the membranes may be depleted, and water dissociation would occur, as may be indicated experimentally by variation of the

measured electrical resistance and pH.

For conventional electrodialysis frames the measured LCD was 6.9 mA/cm^2. A higher value, 8.4 mA/cm^2, was obtained when the 3D printed frames were incorporated along with the internal manifolds. This is a significant increase in LCD, by 21% above the limits of the system. Moreover, the pH was kept more stable throughout the experiments to determine the LCD. This is explained by the more limited and uniform concentration polarization in the electrodialysis cell (see Fig. 5).

The practical utility of additive manufacturing is growing fast, and industrial applications will be seen soon in water desalination. The utilization of better designed manifolds could boost the performance of ED as shown. Furthermore, other electrodialysis variants and other related process where flow distribution plays an important role can be improved, such as electrolysis for hydrogen production, caustic synthesis in the chloralkali process, microbial fuel cells, redox flow batteries, etc. Additionally, novel components such as electrodes, sensors, valves, connectors, mechanical supports, and actuators can be expected to be included in the future into a single piece, adding new functionalities, decreasing the costs and manufacturing complexity, and extending the capabilities of these systems to the next level.

4. Conclusions

Additive manufacturing is able to open new functionalities in designs used for electrodialysis. Internal manifold cavities and hose connectors were successfully integrated into an electrodialysis frame. We show that small changes in hydrodynamic conditions can significantly improve desalination performance. Although the flow distribution is uniform, adoption at industrial conditions remain to be tested, depending on the manufacturer frame design, flowrate, and spacer geometry of the electrodialysis stack. If the fluid velocity is not uniform in the cell, the integration of a manifold and optimization of its design could be implemented, considering a useful range of working flowrates.

Additive manufacturing is presented as an alternative for the manufacture of electrodialysis frames. The size of the frames (and printers), for instance, is a subject that needs to be considered. The results already show great promise for the printed system, which can be adopted not only in industrial desalination but can find use in space exploration, laboratory or household operations that require desalination.

CRediT authorship contribution statement

Conception and design of study: Alvaro Gonzalez-Vogel, Orlando J. Rojas.

Acquisition of data: Alvaro Gonzalez-Vogel, Francisco Felis-Carrasco.

Analysis and/or interpretation of data: Alvaro Gonzalez-Vogel, Francisco Felis-Carrasco.

Drafting the manuscript: Alvaro Gonzalez-Vogel, Francisco Felis-Carrasco, Orlando J. Rojas.

Revising the manuscript critically for important intellectual content: Alvaro Gonzalez-Vogel, Francisco Felis-Carrasco, Orlando J. Rojas.

Approval of the version of the manuscript to be published: Alvaro Gonzalez-Vogel, Francisco Felis-Carrasco, Orlando J. Rojas.

Declaration of competing interest

The authors declare that they have no known competing financial interests or personal relationships that could have appeared to influence the work reported in this paper.

Acknowledgments

The authors are grateful with Arauco Bioforest S.A. for giving the right to use the presented results.

References

[1] D.G. Schniederjans, Adoption of 3D-printing technologies in manufacturing: a survey analysis, Int. J. Prod. Econ. 183 (November 2016) (2017) 287–298.
[2] T. Rayna, L. Striukova, Technological forecasting & social change from rapid prototyping to home fabrication: how 3D printing is changing business model innovation, Technol. Forecast. Soc. Chang. 102 (2016) 214–224.
[3] J.-Y. Lee, et al., The potential to enhance membrane module design with 3D printing technology, J. Memb. Sci. 499 (2016) 480–490.
[4] A. Siddiqui, et al., Development and characterization of 3D-printed feed spacers for spiral wound membrane systems, Water Res. 91 (2016) (2016) 55–67.
[5] F. Li, W. Meindersma, A.B. De Haan, T. Reith, Novel spacers for mass transfer enhancement in membrane separations, J. Memb. Sci. 253 (1–2) (2005) 1–12.
[6] Z.X. Low, Y.T. Chua, B.M. Ray, D. Mattia, I.S. Metcalfe, D.A. Patterson, Perspective on 3D printing of separation membranes and comparison to related unconventional fabrication techniques, J. Memb. Sci. 523 (2017) 596–613.
[7] H. Strathmann, A. Grabowski, and G. Eigenberger, "Electromembrane processes, efficient and versatile tools in a sustainable industrial development," Desalination, vol. 199, no. 1–3, pp. 1–3, Nov. 2006.
[8] J. Balster, D.F. Stamatialis, M. Wessling, Membrane with integrated spacer, J. Memb. Sci. 360 (1–2) (2010) 185–189.
[9] H. Strathmann, Electrodialysis, a mature technology with a multitude of new applications, Desalination 264 (3) (2010) 268–288. Dec.
[10] J. Seo, D.I. Kushner, M.A. Hickner, 3D printing of micro-patterned anion exchange membranes, ACS Appl. Mater. Interfaces (May) (2016), acsami.6b03455.
[11] J. Balster, D.F. Stamatialis, M. Wessling, Multi-layer spacer geometries with improved mass transport, J. Memb. Sci. 282 (2006) 351–361.
[12] P. Xu, M. Capito, and T. Y. Cath, "Selective removal of arsenic and monovalent ions from brackish water reverse osmosis concentrate," J. Hazard. Mater., vol. 260, pp. 885–91, Sep. 2013.
[13] N. Káňavová, L. Machuča, A novel method for limiting current calculation in electrodialysis modules, Period. Polytech. Chem. Eng. 58 (2) (2014) 125–130.
[14] H.-J. Lee, H. Strathmann, and S.-H. Moon, "Determination of the limiting current density in electrodialysis desalination as an empirical function of linear velocity," Desalination, vol. 190, no. 1–3, pp. 43–50, Apr. 2006.
[15] Y. Tanaka, Limiting current density of an ion-exchange membrane and of an electrodialyzer, J. Memb. Sci. 266 (1–2) (2005) 6–17.
[16] D.A. Cowan, J.H. Brown, Effect of turbulence on limiting current in electrodialysis cells, Ind. Eng. Chem. 51 (12) (1959) 1445–1448.